ACS Chemical Neuroscience

Research Article

pubs.acs.org/chemneuro

How Does Hyperphopsphorylation Promote Tau Aggregation and Modulate Filament Structure and Stability?

Liang Xu,[†] Jie Zheng,[‡] Martin Margittai,[§] Ruth Nussinov,[∥,⊥] and Buyong Ma*[,⊥]

[†]School of Chemistry, Dalian University of Technology, Dalian 116024, China

[‡]Department of Chemical & Biomolecular Engineering, The University of Akron, Akron, Ohio 44325, United States

[§]Department of Chemistry and Biochemistry, University of Denver, Denver, Colorado 80208, United States

[∥]Sackler Institute of Molecular Medicine, Department of Human Genetics and Molecular Medicine, Sackler School of Medicine, Tel Aviv University, Tel Aviv 69978, Israel

[⊥]Basic Research Program, Leidos Biomedical Research, Inc., Cancer and Inflammation Program, Frederick National Laboratory for Cancer Research, NCI, Frederick, Maryland 21702, United States

Supporting Information

ABSTRACT: Tau proteins are hyperphosphorylated at common sites in their N- and C-terminal domains in at least three neurodegenerative diseases, Parkinson, dementia with Lewy bodies, and Alzheimer's, suggesting specific pathology but general mechanism. Full-length human tau filament comprises a rigid core and a two-layered fuzzy coat. Tau is categorized into two groups of isoforms, with either four repeats (R1−R4) or three repeats (R1, R3, and R4); their truncated constructs are respectively called K18 and K19. Using multiscale molecular dynamics simulations, we explored the conformational consequences of hyperhposphorylation on tau's repeats. Our lower conformational energy filament models suggest a rigid filament core with a radius of ∼30 to 40 Å and an outer layer with a thickness of ∼140 Å consisting of a double-layered polyelectrolyte. The presence of the phosphorylated terminal domains alters the relative stabilities in the K18 ensemble, thus shifting the populations of the full-length filaments. However, the structure with the straight repeats in the core region is still the most stable, similar to the truncated K18 peptide species without the N- and C-terminus. Our simulations across different scales of resolution consistently reveal that hyperphosphorylation of the two terminal domains decreases the attractive interactions among the N- and C-terminus and repeat domain. To date, the relationship on the conformational level between phosphorylation and aggregation has not been understood. Our results suggest that the exposure of the repeat domain upon hyperphosphorylation could enhance tau filament aggregation. Thus, we discovered that even though these neurodegenerative diseases vary and their associated tau filaments are phosphorylated to different extents, remarkably, the three pathologies appear to share a common tau aggregation mechanism.

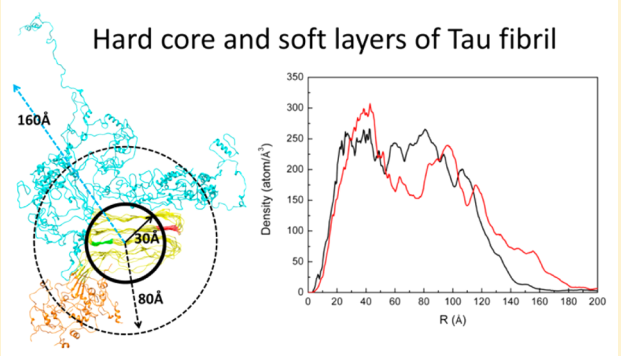

KEYWORDS: *Tau, Alzheimer's disease, amyloid, hyperphosphorylation, paired helical filaments*

Alzheimer's disease (AD) is characterized by the coexistence of the extracellular senile plaques of amyloid-β (Aβ) and the intracellular neurofibrillary tangles of tau protein.[1] In AD, hyperphosphorylated tau proteins are observed in intracellular neurofibrillary tangles in the form of paired helical filaments (PHFs).[2−4] Comprising 352−441 amino acids,[5] the tau protein is one of the largest amyloidogenic proteins that forms complex filaments.[6] Tau is a microtubule-associated protein, which plays important roles in regulating the stability and dynamics of microtubules (MTs), neurite outgrowth, and axonal transport in the normal phosphorylation state.[7,8] The regulation of tau primarily involves post-translational modifications (PTMs) including phosphorylation, truncation, nitration, glycation, acetylation, and methylation.[9−12] The most common tau PTM is phosphorylation. In the AD brain, tau is excessively phosphorylated, at least ∼3-fold over that in normal brain, leading to the disruption of the MTs and the promotion of filament formation.[13] Other PTMs can also regulate tau aggregation; for example, tau truncation may take place after tau hyperphosphorylation with subsequent glycation.[9] Methylation has been shown to suppress tau's aggregation propensity, whereas glycation and acetylation promote pathological tau aggregation.[10,11] Site-specific nitration of residues Tyr18 and Tyr394 significantly decreases tau

Received: November 6, 2015
Accepted: February 8, 2016
Published: February 8, 2016

DOI: 10.1021/acschemneuro.5b00294
ACS Chem. Neurosci. 2016, 7, 565−575

filamentous mass.[12] Although insoluble tau aggregates have long been the focus of efforts to elucidate the mechanism of tau dysfunction and toxicity, recent research suggested that soluble tau oligomers may be responsible for tauopathy.[14−18]

Six tau isoforms have been identified in the adult human brain, with either three or four MT binding repeats (3R or 4R) (Figure 1). These repeated domains are crucial for the binding

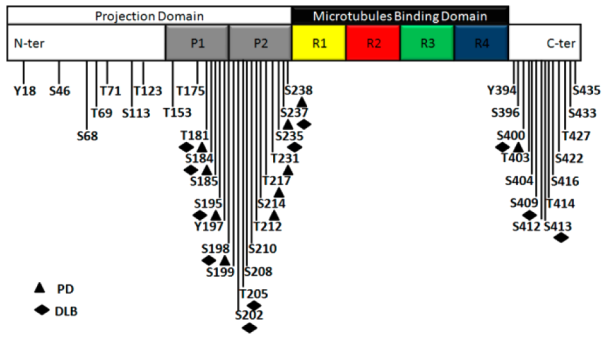

Figure 1. Schematic representation of the largest isoform of tau with specific phosphorylation sites. Two hexapeptides (^{275}VQIINK^{280} and ^{306}VQIVYK^{311}) are in R2 and R3, respectively. Serine, threonine, and tyrosine residues that can be phosphorylated in Alzheimer's disease (AD), Parkinson's disease (PD), and dementia with Lewy bodies (DLB) are indicated.

of tau to the MTs; they also serve in the nucleation of tau aggregation.[19,20] Tau is a natively unfolded protein with a highly polymorphic ensemble.[21] The combination of NMR and molecular simulations revealed that the 4R (four repeats, R1−R4) construct, K18 (comprising residues 244−372), is prone to sample turn conformations.[22,23] Upon aggregation, tau undergoes a conformational transition from mostly random coil to more extended conformations, and this especially holds for two hexapeptide regions (^{275}VQIINK^{280} and ^{306}VQIVYK^{311}) located in repeats 2 (R2) and 3 (R3) that adopt β-sheet structures.[24−26] In the absence of the N- and C-terminal regions, the filaments of the truncated tau constructs K18 (4R domain) and K19 (3R domain) display highly ordered structures,[27,28] with R3 adopting parallel, in-register β-strands.[27−29] The aggregation of tau into filaments has been extensively studied,[30] particularly the core domains of K18 and K19 and the effects of varying conditions on filament stability.[31−40] Tau constructs can self-aggregate to PHFs directly (e.g., when expressed in *E. coli*[41]); however, hyperphosphorylated tau appears to aggregate more readily and may sequester normal tau at lower concentrations.[42,43]

Unlike the truncated constructs, the filament of full-length human tau (htau40) has been suggested to consist of a dense core coated with fuzzy N- and C-terminal regions resembling a double-layered polyelectrolyte brush.[6,44] How the fuzzy coat stabilizes the tau filament is still poorly understood. It has been suggested that the N- and C-terminus differentially associate with PHFs[45] and play distinct roles in the stability and consequently neurotoxicity of tau filaments.[46] The N-terminal fragment (residues 1−15) does not affect tau polymerization,[47] whereas a fragment consisting of residues 1−196 can inhibit polymerization of full-length tau.[48] The side chains of htau40 (residues 272−289) were shown to be able to modulate the tau filament structure.[37] On the other hand, the C-terminal region of tau is crucial in the formation of tau PHFs.[49] However, how the N- and C-terminus of htau40 affect the polymorphic core domain has remained elusive. The distribution of phosphorylation sites along the sequence of full-length tau is uneven. htau40 has 80 serine/threonine and 5 tyrosine residues that can be phosphorylated. Of these 85 residues, 67 are in either the N- or C-terminal regions.[50,51] Early studies of patients' brains indicated that among these the average number of phosphorylated residues is at least 7−8.[52,53] However, mass spectrometry, which is more accurate, identified more sites (36) in purified PHF-tau from human Alzheimer brain than did the early antibody detection method.[54] While each kinase can phosphorylate 10−28 sites in tau, the combination of the four kinases can produce 32 (out of a total of 52 phosphorylation sites when using the kinases separately).[54] Unlike tau phosphorylation sites, the other pathogenic tau PTMs have less established modification sites. For example, ∼11 lysine sites were detected in the MT binding repeat region for tau methylation,[11] and only one lysine (K280) was specifically identified for tau acetylation.[10] It is thus important to understand the effect of phosphorylation on the tau filaments to gain insight into the mechanism of self-assembly of the hyperphosphorylated protein.

Complementary to experimental results from biophysical and biochemical studies, computer simulations are able to characterize the molecular structures and dynamics of tau proteins in solution. Using hard-sphere models, Monte Carlo simulations investigated the effects of phosphorylation on tau aggregation and interactions with MTs.[55] All-atom molecular dynamics (MD) simulations were also carried out to study the conformational changes of phosphorylation on the tau fragment (residues 225−250).[56] Extensive all-atom replica-exchange molecular dynamics (REMD) simulations have recently been performed to examine the structural properties of K18 and K19 in monomeric and oligomeric states.[35,57] REMD simulations also suggested that R3 containing the ^{306}V−K^{317} motif displays a much stronger propensity to aggregate than does R2 containing ^{273}G−L^{284}.[58] However, few simulations have been performed to investigate the structure and dynamics of full-length tau proteins and the interactions of the fuzzy coat with the core domain. In this work, we performed multiscale MD simulations (Figure 2) to study the structure and dynamics of

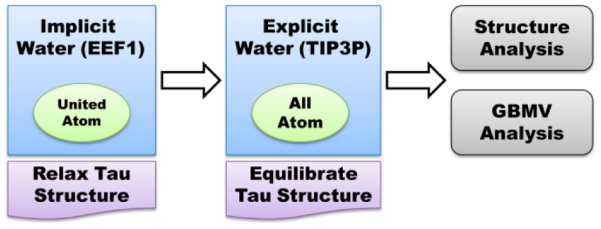

Figure 2. Flowchart of multiscale MD simulations of tau filaments.

full-length tau filaments, especially the effects of the flanking regions on the stability of the filament core (Figure 3). We found that full-length tau filaments consist of one dense core and two sparse layers, consistent with the structural model derived from the experimental observations. The relative stability of the filaments not only depends on the core morphology but also can shift by interactions among different domains. As expected, phosphorylation events in the flanking regions alter the distribution of mass and charge throughout the filaments. There are significant domain movements within the tau filament core, which becomes less dense and less structured

DOI: 10.1021/acschemneuro.5b00294
ACS Chem. Neurosci. 2016, 7, 565−575

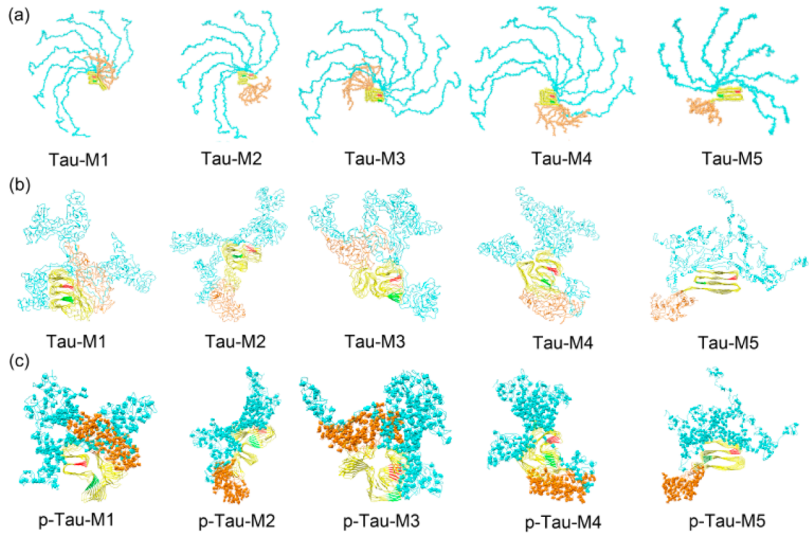

Figure 3. Representative conformations for different normal and hyperphosphorylated tau filaments. (a) Initial conformations used in self-guided Langevin dynamics with the EEF1 solvent model. (b) Equilibrated conformations for tau filaments. (c) Hyperphosphorylated tau filaments. The N-terminus, repeat domain, and C-terminus of tau filaments are shown in cyan, yellow, and orange, respectively. Two hexapeptides (^{275}VQIINK^{280} and ^{306}VQIVYK^{311}) are shown in red and green, respectively. Phosphorylated serine, threonine, tyrosine residues in both the N- and C-terminus are also shown as spheres.

and more exposed to the solvent environment, especially R2 and R3. The protrusion of R2/R3 from the core of tau filaments facilitates further aggregation.

RESULTS AND DISCUSSION

Relative Stability of Full-Length Tau Filaments. The conformation energy based on the generalized Born using the molecular volume (GBMV) method was first calculated for the conformations of normal tau filaments (Figure 4a). These filaments were subjected to self-guided Langevin dynamics (SGLD) simulations with the EEF1 implicit solvent model (160 ns each, Figure S1; see Methods), followed by all-atom MD simulations (20 ns each) (Figure 5a). The conformational energy suggests that Tau-M5 is the most stable filament and that Tau-M3 is the least stable. Note that the core of Tau-M5 corresponds to the truncated K18-9 (SL, straight-line, shape) in previous studies, which is the most energetically favorable model among all K18 filaments that we examined.[40] In addition, the truncated K18 in Tau-M2 is the least stable model (corresponding to K18-6 in previous studies), whereas full-length Tau-M2 is the second most stable filament among the five models studied here. This result indicates that the presence of both terminals has a significant effect on the relative stability of full-length tau filaments and thus their relative populations. It has been shown that human tau isoforms assemble into polymorphic fibrils with different stabilities.[59] In one report, the ratios of thick to thin fibrils for different isoforms were 2:3, 3:1, 1:4, and 1:1 for hTau40, hTau23, K18, and K19, respectively.[59] Computational modeling revealed that there are large population differences among the polymorphic structures for K18,[40] which may correspond to the large 1:4 ratio of thick to thin fibrils for K18. Our current study indicated that the energy differences among the different tested structures are relatively small (Figure 4a), which could be related to the lower 2:3 ratio of thick to thin fibrils for hTau40.

Mass and Charge Distribution of Tau Filaments. We calculated the cumulative mass and charge density distributions from the center of the tau fibril core for each filament model (Figure 6). The geometrical center of the 4R domain (residues 243−372) was set as the origin. Although various mass distribution diagrams were obtained, the density decreases to zero at about 160−180 Å, suggesting that all tau filament models have a rough radius of ∼160 to ∼180 Å. Except for Tau-M1 and Tau-M5, whose 4R domains deviate markedly from a globular shape, the other three filament models display a density peak at ∼30 to 40 Å, indicating the existence of a dense filament core with a radius of ∼30 to 40 Å. As a result, the tau filament's termini have a thickness of ∼130 to 150 Å. These results are generally consistent with atomic force microscopy observations of full-length tau fibrils, which suggest that the radius of the tau fibril core is ∼30 to 33 Å and the thickness of tau's termini is ∼130 to 160 Å. In the case of Tau-M1, the radius of the tau core extends up to ∼50 Å. For Tau-M5, although its R3 displays a straight-line shape, it also has a radius of ∼30 Å for the fibril core. The other density peaks shown in Figure 6a are attributed to tau's termini, which are the least pronounced in the Tau-M1 model where the mass density decreases almost monotonically. In addition to the position where the mass density reaches zero (∼180 Å from the core), Tau-M2 and Tau-M5 exhibit another density maximum with radii of ∼80 and 90 Å from the core. In the case of Tau-M3 and Tau-M4, however, the second mass peak either extends to 100 Å or shrinks to 60 Å. The above results suggest that tau filaments may consist of two layers with distinct radii. On the basis of the mass density of Tau-M2 and Tau-M5, the thicknesses are ∼50 and 100 Å for the first and second sparse layers surrounding the rigid core. However, a thickness of up to ∼80 Å was suggested for each fuzzy layer of the tau fibril. In addition, both Tau-M2 and Tau-M5 display a thickness of 150 Å for the outer layer, which is close to the value of ∼160 Å observed experimentally.[6]

The distribution of the radius of charge density (Figure 6b) displays a very similar pattern for various tau filament models, with positive and negative charge distributions separated from each other along the tau filaments. The positive charge density spreads from the core up to a radius of ∼60 to ∼70 Å for all

DOI: 10.1021/acschemneuro.5b00294
ACS Chem. Neurosci. 2016, 7, 565−575

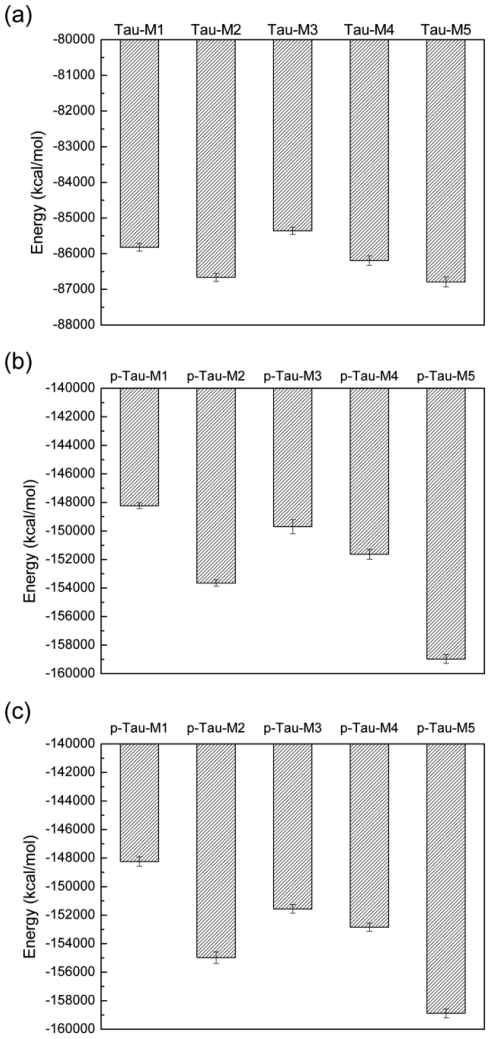

Figure 4. Conformational energy (GBMV) of normal and hyperphosphorylated tau filaments. All calculations are based on all-atom MD simulations in explicit water. (a) Conformational energy of normal tau filament with starting structures as shown in Figure 3b. (b) Conformational energy of hyperphosphorylated tau filaments with starting conformations similar to those shown in Figure 3b. (c) Conformational energy of hyperphosphorylated tau filaments with starting conformations as shown in Figure 3c.

models. As the core has a thickness of ∼30 to 40 Å in the simulated filaments, the two-layered termini of the filaments have distinct electrostatics. For example, the first layer of Tau-M2's termini has ∼10 Å thick positive and ∼30 Å thick negative charge distributions, whereas the second layer has only a ∼100 Å thick negative charge distribution. Due to the polymorphic conformations of tau termini, the positions of the maximum negative value in the second layer vary among tau filaments. In Tau-M2, Tau-M3, and Tau-M4, the positive charge distribution reaches a maximum at ∼40 Å from the core. The maximum shifts to ∼50 Å in Tau-M1 and 30 Å in Tau-M5. The electrostatic distributions in the filament models are consistent with the experimentally derived two-layered polyelectrolyte brush model. Moreover, compared with the dominant electrostatic repulsion between the two layers, the concurrence of both electrostatic attraction and repulsion between the tau filament core and the first layer of the termini makes the first layer more compact and the second layer more sparse, which in turn contributes to different mechanical properties of the filament's termini, as observed in experiments.[6]

Interactions between Different Domains of Tau Filaments. To investigate the effects of termini on the stability of tau filaments, we calculated the interaction energies between the N-terminal domain (ND, residues 1−242), repeat domain (RD, residues 243−372), and C-terminal domain (CD, residues 373−441). Because tau is highly hydrophilic, the electrostatic interaction energies contribute about 6−7 times more than the van der Waals interactions. As shown in Figure 7, the most significant difference in the interaction energy is between ND and CD in different tau filaments. For example, Tau-M1 and Tau-M5 display comparable interaction energies between ND and RD and between RD and CD; however, Tau-M1 shows the most favorable interaction energy (approximately −4648 kcal/mol) between ND and CD, but such interaction energy is only approximately −253 kcal/mol in Tau-M5 due to the clear separation between ND and CD by RD. It seems that the interactions between ND and CD may contribute significantly to the stability of Tau-M1. However, the above interaction energies were calculated in vacuum, whereas the conformational energy in terms of GBMV takes the solvent effect into account. As a result, the contribution of the interaction between ND and CD of Tau-M1 in the presence of solvent could be less significant. Nevertheless, our results corroborate an earlier study where the N-terminal region of tau interacted with the C-terminal region (residues 392−421), thereby inhibiting tau

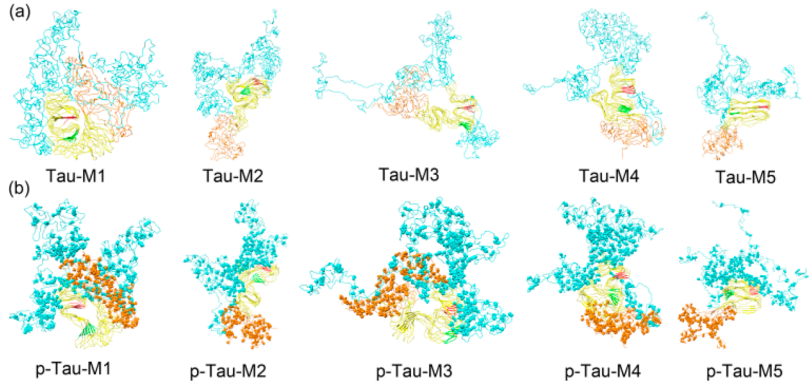

Figure 5. (a) Representative conformations of tau filaments after 20 ns all-atom MD simulations. The starting conformations are the same as those shown in Figure 3b. (b) Representative conformations of hyperphosphorylated tau filaments after 20 ns all-atom MD simulations. The starting conformations are the same as those shown in Figure 3c.

DOI: 10.1021/acschemneuro.5b00294
ACS Chem. Neurosci. 2016, 7, 565−575

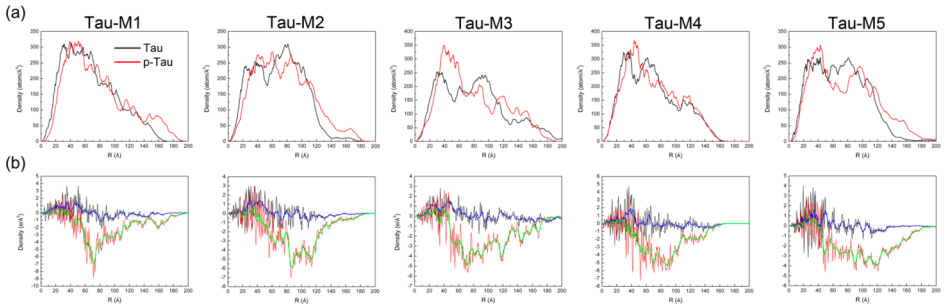

Figure 6. Cumulative mass and charge density distributions from the center of the tau fibril's core reflect tau filament dimensions. (a) Radius distribution of mass density of tau (black) and hyperphosphorylated tau (red) filaments for different structural models. (b) Radius distribution of charge density along tau (black) and hyperphosphorylated tau (red) filaments for different structural models. The blue and green lines are smoothing lines based on an adjacent average.

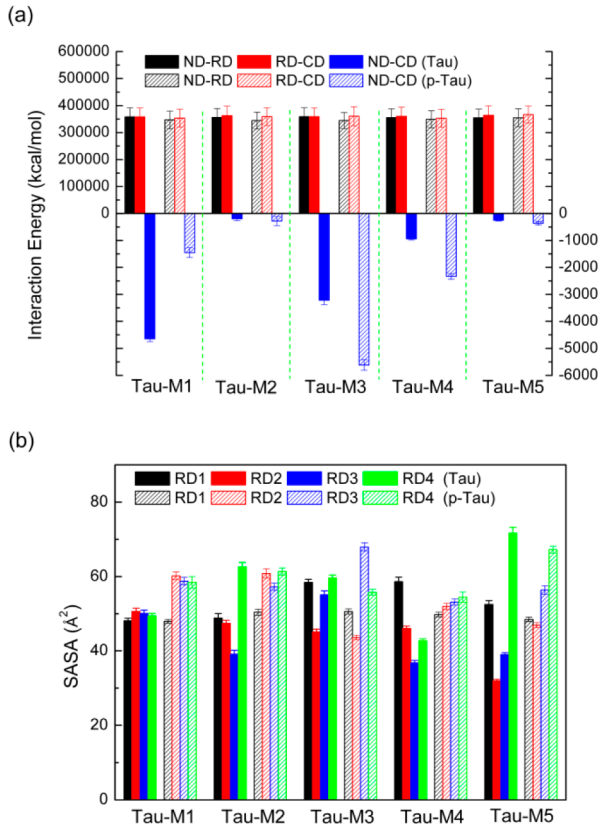

Figure 7. (a) Interaction energies among N-terminal domain (ND), C-terminal domain (CD), and repeat domain (RD) of tau and hyperphosphorylated tau filaments. (b) SASA of each RD of tau and hyperphosphorylated tau filaments, which has been normalized by the number of residues in each repeat for each monomer.

filament formation.[60] We observed that Tau-M3 and Tau-M5 are relatively more stable than the other tau filaments (Figure 4), whereas they have unfavorable interactions between the ND and CD (Figure 7). Such results also highlight the important role of water molecules in the stability of tau aggregates.

Effects of Hyperphosphorylated Termini on Tau Filaments. While the average concentration is at least around 7−8 phosphorylated residues distributed among these potential phosphorylation sites,[52,53] many more sites are possible.[54] We tested the extreme cases where most observed sites are phosphorylated. We selectively phosphorylated a total of 41 residues in the termini of the filaments (Figure 1). Tau phosphorylation on sites preceding to S208 primarily suppresses aggregation but enhances tau aggregation in the C-terminal region.[9] This led us to examine these two opposing effects on the stability of full-length tau filaments. The starting conformations used in the first set of MD simulations of phosphorylated filaments in an explicit solvent environment were taken from the conformations at 120 ns of simulations using the EEF1-SGLD protocol (Figure 2b). After 20 ns MD simulations, except for phosphorylated Tau-M4 (p-Tau-M4), no significant conformational changes were observed (Figure S2). However, comparing the RD (K18) portion of the core region of the filaments revealed that phosphorylation leads to smaller RMSD for most models, except p-Tau-M5 (Figure S3). Overall, the RMSDs of the K18 region in full-length tau are smaller than those for the isolated K18 peptide (except K18-7), and hyperphosphorylation further consolidated the structural stabilities of the tau filament core. The conformational energy in terms of the GBMV implies that p-Tau-M5 is the most energetically favorable (Figure 4b), followed by p-Tau-M2. We also found that phosphorylation of both termini alters the relative stabilities of p-Tau-M1 and p-Tau-M3 (Figure 4a,b).

To accelerate the conformational sampling, these p-Tau filaments were first subjected to 40 ns SGLD simulations with the EEF1 solvent model, and representative conformations are shown in Figure 3c. All p-Tau filaments display significant conformational changes. To test if these conformations are still stable under explicit solvent conditions, all-atom MD simulations in explicit water were subsequently performed. The final conformations after 20 ns simulations are shown in Figure 5b. We found that all p-Tau filaments retained the same conformations as those from the implicit solvent MD simulations (Figures 3c and 5b), indicating that conformations sampled in either implicit or explicit solvent are accessible by tau filaments phosphorylated at both termini.

The conformational energy of these p-Tau filaments shows the same trend as that in the first set of MD simulations (Figure 4b,c), confirming that p-Tau-M5 is the most stable model. The introduction of too many negative charges due to phosphorylation changed the density distribution of the fibrils. The mass density shown in Figure 6a suggests that the thickness increases. A 5−10 Å expansion of the core radius was observed in the p-Tau filaments. Noticeably, the density of the first outer layer increases, but the density of the second layer decreases, implying that the first layer of tau termini becomes much denser, whereas the second layer becomes much sparser. The structural alterations can be rationalized in terms of the charge density along the p-Tau filaments (Figure 6b). In contrast to the positive charge distribution in the core region, the zero to

DOI: 10.1021/acschemneuro.5b00294
ACS Chem. Neurosci. 2016, 7, 565−575

negative charge distribution in the same region clearly indicates the overlap of phosphorylated termini with the core domain. The electrostatic attraction between the core region and the termini results in a more compact and thus denser region within the p-Tau filaments. On the other hand, the electrostatic repulsion leads to a sparer outer region (Figure 5b).

The above structural changes are also reflected in the calculated interaction energies (Figure 7a). Interestingly, no significant difference was observed in the interactions between CD and RD and between ND with RD for various p-Tau filaments. Due to the hyperphosphorylation sites in both ND and CD, the interactions between them should become less preferred accordingly. However, only p-Tau-M1 displays such unfavorable interactions, and the other p-Tau filaments demonstrate either no significant change in the interaction energies between ND and CD (p-Tau-M2 and p-Tau-M5) or even preferred interactions (p-Tau-M3 and p-Tau-M4) compared with those of their normal species. The structure of the RD was disturbed significantly due to the hyperphosphorylation in the termini, which not only affected the interactions between ND/CD and RD but also simultaneously influenced the interactions between ND and CD. To follow the conformational changes of RD in the p-Tau filaments, we calculated the solvent-accessible surface area (SASA) for each RD (Figure 7b). Compared to normal tau filaments, the SASA of R2 and R3 in p-Tau-M2 increases ∼28 and ∼46%, respectively. In p-Tau-M5, the SASA of R2 and R3 also increases ∼47 and 44%, respectively. Except for p-Tau-M3, the other less stable p-Tau filaments display an increase in the SASA for R2 and R3 to various extents. For example, p-Tau-M1 shows an increase in SASA of R2 and R3 by ∼19 and 17%, respectively. As for R1 and R4, they are either buried inside the protein or exposed to the solvent, with the alterations in SASA dependent on the specific tau filaments. In most phosphorylated models, without the edge strands, the RD portions have smaller RMSDs (Figure S3). The edge strands contributed the most to the increase in SASA. In summary, the general increase in SASA of R2 and R3 suggests that the edge strands of RD are more exposed to solvent, which may promote p-Tau filament aggregation in aqueous solution.

The 41 phosphorylation sites in AD present different patterns of overlap with PD and dementia with Lewy bodies (DLB).[61] In the striatum of PD, there are 10 tau sites that show considerable hyperphosphorylation, and there are 11 sites that display an increase in phosphorylation in DLB (Figure 1). To test if the different number of phosphorylation sites identified in different brain regions in PD and DLB have the same influence on tau filaments as we found in AD, the same initial conformation of Tau-M1 was used to generate phosphorylated tau filaments with 10 or 11 phosphorylation sites individually. As shown in Figure 8, p-Tau-M1 filaments in these diseases show a similar distribution of mass density. A slight decrease and increase in mass density at ∼100 and ∼150 Å were also found, resulting in different conformations. The distribution of charge density also exhibits a similar trend in PD and DLB, although they have only six phosphorylation sites in common (Figure 8b). Interestingly, the significant difference in the negative charge of p-Tau between AD and PD/DLB does not shift the density minimum at ∼70−80 Å from the core, suggesting the formation of two-layered polyelectrolyte termini of p-Tau in both PD and DLB. We did not observe a significant difference in the interaction energy of p-Tau between PD and DLB; however, the interactions between ND and CD became

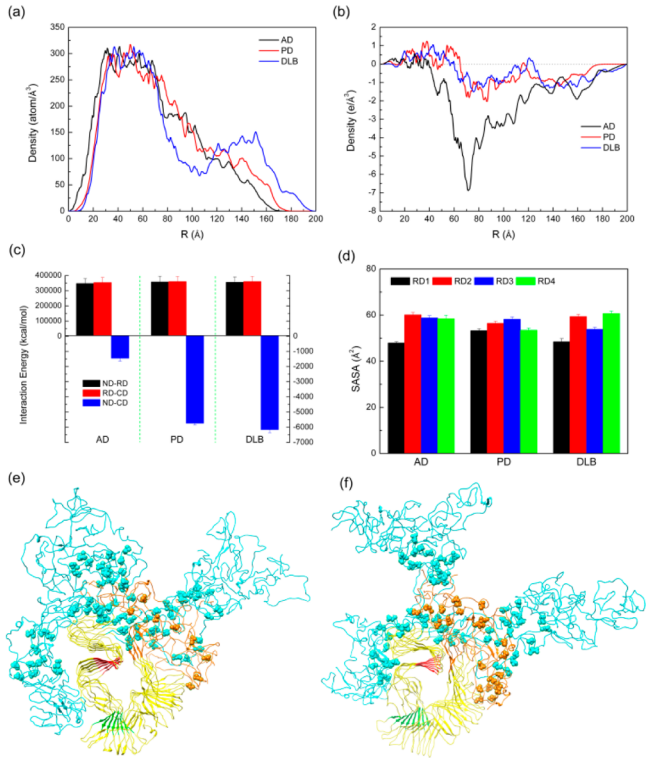

Figure 8. (a, b) Radius distribution of mass and charge density of p-Tau-M1 filament in AD, PD, and DLB. (c) Interaction energies among ND, RD, and CD of p-Tau-M1 in AD, PD, and DLB. (d) Normalized SASA of each RD of p-Tau-M1 in AD, PD, and DLB. (e, f) Representative conformations of p-Tau-M1 filaments in PD (e) and DLB (f).

more favorable compared to those of p-Tau in AD (Figure 8c). Moreover, p-Tau-M1 filaments in different diseases demonstrate very similar RD SASAs (Figure 8d). Thus, our results imply that tau filaments with a different number of phosphorylation sites in AD, PD, and DLB may have the same effect on the structure and stability of normal tau filaments (Figure 8e−f), confirming the experimental observations that the formation of p-Tau may be a common denominator in these three neurodegenerative diseases.[61−63]

It has been well-known that the RD alone aggregates into filaments more readily than full-length tau.[30] Previous studies showed that R2 and R3, which contain two important hexapeptide regions (^{275}VQIINK^{280} and ^{306}VQIVYK^{311}), display strong aggregation propensities.[58,64] A recent simulation study suggested that the Aβ42 protofibril interacts with monomeric K18 and K19 and exposes the two hexapeptide motifs.[65] In addition, cofactors such as polyanions (e.g., heparin) promote tau aggregation.[66] Although hyperphosphorylated tau is the major component of neurofibrillary tangles, the effect of hyperphosphorylation on the aggregation mechanism has not been well-elucidated on the molecular level. Here, we found that if tau filaments were hyperphosphorylated in the termini to various degrees then the RD, in particular, R2/R3, becomes more solvent accessible. As a consequence, these regions may better serve as seeds, and their interactions could facilitate the aggregation of p-Tau filaments.

CONCLUSIONS

In this study, we performed multiscale simulations to investigate the structural dynamics of full-length tau filaments

DOI: 10.1021/acschemneuro.5b00294
ACS Chem. Neurosci. 2016, 7, 565−575

as well as the effects of hyperphosphorylated termini on tau filaments. To explore the polymorphic nature of the filaments, various structural models were constructed consisting of an ordered core and unstructured termini. Our results show that the presence of both the N- and C-terminus alters the structure of RD to varying degrees, which in turn shifts the relative stabilities of different tau filaments. The modulation of the tau filaments' stability by the N- and C-terminus was studied by Binder and co-workers.[60,67−75] The C-terminus inhibits tau assembly by interacting with residues 321−375 in the MT binding repeat region.[69] The effects of the N-terminus are more complex. While the isolated N-terminal tau fragments inhibit tau polymerization by interacting with a specific C-terminal sequence, thereby stabilizing a soluble conformation of tau,[60,72] removal of the N-terminus inhibits tau polymerization, reducing both the rate and extent of polymerization.[75] The contribution of the N-terminus to tau polymerization is similar to that by the shorter N-terminus Aβ peptide. Recently, we have demonstrated allosteric stabilization of the amyloid-β peptide hairpin by the fluctuating N-terminal.[68] It has been shown that the conformational changes and truncation of tau occur after its phosphorylation.[73] While these works focused on monomeric mechanisms and indicated that phosphorylation is coupled with enhanced aggregation for molecules with truncated termini, our study indicated that hyperphosphorylation would affect filament states as well. Still, the structure with the straight repeats in the core region is the most stable, similar to the truncated K18 peptide species without the N- and C-terminus. The interactions between ND/CD and RD lead to diverse mass and charge distributions but with the common theme of a two-layered polyelectrolyte sparse coat surrounding a dense core, in agreement with experimental observations. We found that the interactions between ND and CD contribute to the stability of tau filaments. Upon hyperphosphorylation in both termini, electrostatic attraction between RD and ND and electrostatic repulsion between ND and CD cause the expansion of the dense core region and the first and second layers existing in the normal tau filaments. Of importance, our results show that RD undergoes significant structural changes and becomes more solvent accessible. The exposure of the two repeats, R2 and R3, which have high aggregation propensity, may help to recruit additional monomers in amyloid growth. Thus, consistent with previous finding that tau's C-terminus inhibits assembly, this inhibition can be partially reversed by site-specific phosphorylation.[67]

Collectively, our results provide new insights into the aggregation mechanism of tau filaments induced by hyperphosphorylation at both termini.

METHODS

Hybrid-Resolution MD Simulations. Full-length tau filaments were constructed by linking both N- and C-terminal fragments to the structural models of K18 (Figure 3a). Previous experiments and MD simulations have shown that these models are representative isoforms of truncated tau filaments.[31−40] Five K18 octamer filaments were considered in this work, corresponding to K18-2, K18-6, K18-7, K18-8, and K18-9 in previous works.[40] In a study of tau's seeding barrier, based on R3's conformations, three of them, K18-6, K18-8, and K18-9, were referred to as U-shape, L-shape, and SL shape, respectively.[39] For consistency with the K18 filament's (octamer) geometry and to avoid atomic clashes among the terminal residues, steered MD simulations were performed to render both termini in extended conformations. These five filament models (referred to as Tau-M1, Tau-M2, Tau-M3, Tau-M4, and Tau-M5) have a radius of gyration varying from 183 to 191 Å, making MD simulations with an explicit solvent model prohibitive. To address this issue, we performed multiscale MD simulations. First, hybrid-resolution MD simulations were applied to relax these filaments. We used hybrid PACE force field parameters, in which the protein was represented by a united-atom force field and the solvent was represented by the MARTINI coarse-grained water model.[76−78] This approach has been successfully applied in studies of protein folding and Aβ fibril elongation.[79,80] Here, each tau filament was modeled using the PACE force field parameters, solvated in a rectangular water box filled with MARTINI water molecules, and neutralized by adding 16 Na^+. The direction of the filament's elongation axis was not solvated, mimicking the infinite length of tau filaments at a molecular level. The distance between water molecules to protein atoms was set at 12 Å. Three-dimensional periodic boundary conditions were applied with a typical simulation time step of 4 ps.[81] Each system was energy minimized for 5000 steps and heated at 330 K for an additional 5000 steps (20 ps). The modified NAMD program was used to run all simulations.[82]

MD Simulations with Implicit Solvent Model EEF1. We found that such a large system containing 29 488 protein atoms and ∼250 000 MARTINI water molecules is still not able to relax the extended N- and C-terminal conformations. To accelerate the convergence of the simulations, the implicit solvent model EEF1 was used with the CHARMM 19 united-atom force field to model these tau filaments in a solvent environment.[83−85] The starting conformations used in EEF1 simulations were randomly chosen from the last 10 ns conformations of the above PACE simulations. A planar harmonic constraint with a force constant of 100 kcal/mol·Å^2 was applied along the tau filament's axis to model the infinite length. Each system was first energy minimized for 5000 steps and then heated at 300 K for 10 000 steps with a time step of 0.1 fs. SGLD simulations were applied to efficiently search the conformational space of the N- and C-terminus around the filaments.[86,87] An integration time step of 2 fs was used, and a friction constant of 1/ps was set throughout the simulations. We found that each system reaches equilibrium over 120 ns of SGLD simulations (Figure S1). Then, the conformations at 120 ns were used to prepare the starting structures of tau filaments phosphorylated at both the N- and C-terminus. For Tau-M5, we observed that the fold of the core was significantly disrupted; therefore, a conformation earlier than 120 ns was used. A total of 41 residues including 3 tyrosines, 25 serines, and 13 threonines were phosphorylated in the hyperphosphorylated tau simulations (Figure 1). These phosphorylation sites have different extents of overlap across AD, PD, and DLB.[61] The force field parameters for phosphorylated residues were adapted from CHARMM 36 force fields,[88] and the solvation parameters used in EEF1 were taken from previous studies.[89] The hyperphosphorylated tau filaments were simulated for 40 ns under the simulation protocol described above. For comparison, the simulations of normal tau filaments were also extended for an additional 40 ns, leading to a total simulation time of 160 ns for each system. The implicit solvent EEF1/SGLD simulations were carried out using CHARMM (version c35b5).[90]

All-Atom MD Simulations with Explicit Water Molecules. The role of water in amyloid aggregation has been studied previously. Water can accelerate the formation of amyloid fibrils where hydrophobic residues are predominant or slow fibril growth rate by stabilizing metastable intermediates in the case where hydrophilic residues are predominant.[91,92] Although the amino acids in tau protein are hydrophilic overall, the low content of hydrophobic residues seems to be sufficient to drive tau aggregation.[93] To investigate the effect of water on the stability of tau fibrils and to compare this with results obtained using the implicit solvent model of EEF1, all-atom MD simulations with explicit water were also performed. The CHARMM 27 force field including the CMAP correction was used to represent these tau fibrils.[94,95] The water molecules were represented by the TIP3P water model.[96] Similar to the hybrid-resolution MD simulations, the direction of the filament's elongation axis was not solvated, and the minimal distance between tau protein and the boundary of the water box was at least 20 Å. Na^+ ions were added to neutralize each system. The total number of atoms varied from

DOI: 10.1021/acschemneuro.5b00294
ACS Chem. Neurosci. 2016, 7, 565−575

290 961 to 473 528. The PME method was used to treat long-range electrostatic interactions. Periodic boundary conditions were applied for each system. Hydrogen bonds were constrained using the SHAKE algorithm. The van der Waals interactions were calculated using a switching function with a twin cutoff of 10 and 12 Å. An integration time step of 2 fs was used, and the trajectory was saved every 10 ps. Three sets of all-atom MD simulations were performed with different starting structures taken from the above implicit MD simulations. The initial structures used in the first set of simulations were taken from the conformations at 160 ns of the EEF1 simulation of normal tau fibrils (Figure 3b). The starting structures in the other two all-atom MD simulations were taken from the beginning and last conformations of the hyperphosphorylated fibrils used in the EEF1 simulations. The beginning conformations are similar to those shown in Figure 2b but with tyrosines, serines, and threonines in both the N- and C-terminus phosphorylated. The last conformations of the hyperphosphorylated fibrils used for the all-atom MD simulations are shown in Figure 3c. The all-atom MD simulations were performed using NAMD 2 software.[97]

The relative stability of each fibril model was evaluated in terms of the conformational energy calculated by the GBMV method implemented in the CHARMM program (c35b5).[98,99] The standard parameters in the GBMV II algorithm were used. A single-point energy calculation with infinite cutoffs was performed after the structure was minimized by 200 steps of the steepest decent method. For each system, a total of 500 conformations extracted from the last 5 ns trajectory were used to obtain the average energy and for analyses. Note that the conformational energy in terms of the GBMV method was calculated only for those conformations obtained by all-atom MD simulations.

■ ASSOCIATED CONTENT

Supporting Information

The Supporting Information is available free of charge on the ACS Publications website at DOI: 10.1021/acschemneuro.5b00294.

Radius of gyration of tau filaments based on the SGLD simulations with the EEF1 implicit solvent model (Figure S1); representative conformations of hyperphosphorylated tau filaments after 20 ns all-atom MD simulations (Figure S2); and backbone RMSD of tau and hyperphosphorylated tau filaments (Figure S3) (PDF)

■ AUTHOR INFORMATION

Corresponding Author

*E-mail: mabuyong@mail.nih.gov. Phone: (301) 846-6540.

Funding

This project was funded in whole or in part with Federal funds from the National Cancer Institute, National Institutes of Health, under contract number HHSN261200800001E. This research was supported (in part) by the Intramural Research Program of the NIH, National Cancer Institute, Center for Cancer Research. L.X. thanks the China Scholarship Council (CSC201306065001) for financial support. J.Z. thanks the NSF (CAREER Awards CBET-0952624 and CBET-1510099) and Alzheimer Association, New Investigator Research Grant (2015-NIRG-341372), for financial support. This project was supported by National Institute of Neurological Disorders and Stroke Grant R01NS076619 (to M.M.).

Notes

The authors declare no competing financial interest.

■ ACKNOWLEDGMENTS

MD simulations were performed at the high-performance computational facilities of the Biowulf PC/Linux cluster at the NIH (http://biowulf.nih.gov/).

■ REFERENCES

(1) Hardy, J. A., and Higgins, G. A. (1992) Alzheimer's disease: the amyloid cascade hypothesis. *Science 256*, 184−185.

(2) Morris, M., Maeda, S., Vossel, K., and Mucke, L. (2011) The Many Faces of Tau. *Neuron 70*, 410−426.

(3) Ramachandran, G., and Udgaonkar, J. B. (2013) Mechanistic Studies Unravel the Complexity Inherent in Tau Aggregation Leading to Alzheimer's Disease and the Tauopathies. *Biochemistry 52*, 4107−4126.

(4) Fontaine, S. N., Sabbagh, J. J., Baker, J., Martinez-Licha, C. R., Darling, A., and Dickey, C. A. (2015) Cellular factors modulating the mechanism of tau protein aggregation. *Cell. Mol. Life Sci. 72*, 1863−1879.

(5) Kolarova, M., García-Sierra, F., Bartos, A., Ricny, J., and Ripova, D. (2012) Structure and Pathology of Tau Protein in Alzheimer Disease. *Int. J. Alzheimer's Dis. 2012*, 1−13.

(6) Wegmann, S., Medalsy, I. D., Mandelkow, E., and Muller, D. J. (2013) The fuzzy coat of pathological human Tau fibrils is a two-layered polyelectrolyte brush. *Proc. Natl. Acad. Sci. U. S. A. 110*, E313−E321.

(7) Ballatore, C., Lee, V. M. Y., and Trojanowski, J. Q. (2007) Tau-mediated neurodegeneration in Alzheimer's disease and related disorders. *Nat. Rev. Neurosci. 8*, 663−672.

(8) Bhatia, N., and Hall, G. (2013) Untangling the role of tau in Alzheimer's disease: A unifying hypothesis. *Translational Neuroscience 4*, 115−133.

(9) Martin, L., Latypova, X., and Terro, F. (2011) Post-translational modifications of tau protein: Implications for Alzheimer's disease. *Neurochem. Int. 58*, 458−471.

(10) Cohen, T. J., Guo, J. L., Hurtado, D. E., Kwong, L. K., Mills, I. P., Trojanowski, J. Q., and Lee, V. M. Y. (2011) The acetylation of tau inhibits its function and promotes pathological tau aggregation. *Nat. Commun. 2*, 252.

(11) Funk, K. E., Thomas, S. N., Schafer, K. N., Cooper, G. L., Liao, Z., Clark, D. J., Yang, A. J., and Kuret, J. (2014) Lysine methylation is an endogenous post-translational modification of tau protein in human brain and a modulator of aggregation propensity. *Biochem. J. 462*, 77−88.

(12) Reynolds, M. R., Berry, R. W., and Binder, L. I. (2005) Site-specific nitration differentially influences tau assembly in vitro. *Biochemistry 44*, 13997−14009.

(13) Johnson, G. V. W., and Stoothoff, W. H. (2004) Tau phosphorylation in neuronal cell function and dysfunction. *J. Cell Sci. 117*, 5721−5729.

(14) Ward, S. M., Himmelstein, D. S., Lancia, J. K., and Binder, L. I. (2012) Tau oligomers and tau toxicity in neurodegenerative disease. *Biochem. Soc. Trans. 40*, 667−671.

(15) Cowan, C. M., Quraishe, S., and Mudher, A. (2012) What is the pathological significance of tau oligomers? *Biochem. Soc. Trans. 40*, 693−697.

(16) Gerson, J. E., Castillo-Carranza, D. L., and Kayed, R. (2014) Advances in Therapeutics for Neurodegenerative Tauopathies: Moving toward the Specific Targeting of the Most Toxic Tau Species. *ACS Chem. Neurosci. 5*, 752−769.

(17) Maeda, S., Sahara, N., Saito, Y., Murayama, M., Yoshiike, Y., Kim, H., Miyasaka, T., Murayama, S., Ikai, A., and Takashima, A. (2007) Granular Tau Oligomers as Intermediates of Tau Filaments†. *Biochemistry 46*, 3856−3861.

(18) Shammas, S. L., Garcia, G. A., Kumar, S., Kjaergaard, M., Horrocks, M. H., Shivji, N., Mandelkow, E., Knowles, T. P. J., Mandelkow, E., and Klenerman, D. (2015) A mechanistic model of tau amyloid aggregation based on direct observation of oligomers. *Nat. Commun. 6*, 7025.

DOI: 10.1021/acschemneuro.5b00294
ACS Chem. Neurosci. 2016, 7, 565−575

(19) Mylonas, E., Hascher, A., Bernadó, P., Blackledge, M., Mandelkow, E., and Svergun, D. I. (2008) Domain Conformation of Tau Protein Studied by Solution Small-Angle X-ray Scattering†. *Biochemistry 47*, 10345−10353.
(20) Goode, B. L. (2000) Structural and Functional Differences between 3-Repeat and 4-Repeat Tau Isoforms. Implications for Normal Tau Function and the Onset of Neurodegenerative Disease. *J. Biol. Chem. 275*, 38182−38189.
(21) Petsko, G. A., Mukrasch, M. D., Bibow, S., Korukottu, J., Jeganathan, S., Biernat, J., Griesinger, C., Mandelkow, E., and Zweckstetter, M. (2009) Structural Polymorphism of 441-Residue Tau at Single Residue Resolution. *PLoS Biol. 7*, e34.
(22) Mukrasch, M. D., Markwick, P., Biernat, J., von Bergen, M., Bernado, P., Griesinger, C., Mandelkow, E., Zweckstetter, M., and Blackledge, M. (2007) Highly populated turn conformations in natively unfolded tau protein identified from residual dipolar couplings and molecular simulation. *J. Am. Chem. Soc. 129*, 5235−5243.
(23) Luo, Y., Ma, B., Nussinov, R., and Wei, G. (2014) Structural Insight into Tau Protein's Paradox of Intrinsically Disordered Behavior, Self-Acetylation Activity, and Aggregation. *J. Phys. Chem. Lett. 5*, 3026−3031.
(24) von Bergen, M., Barghorn, S., Biernat, J., Mandelkow, E.-M., and Mandelkow, E. (2005) Tau aggregation is driven by a transition from random coil to beta sheet structure. *Biochim. Biophys. Acta, Mol. Basis Dis. 1739*, 158−166.
(25) Ramachandran, G., Milán-Garcés, E. A., Udgaonkar, J. B., and Puranik, M. (2014) Resonance Raman Spectroscopic Measurements Delineate the Structural Changes that Occur during Tau Fibril Formation. *Biochemistry 53*, 6550−6565.
(26) Jeganathan, S., von Bergen, M., Mandelkow, E.-M., and Mandelkow, E. (2008) The Natively Unfolded Character of Tau and Its Aggregation to Alzheimer-like Paired Helical Filaments†. *Biochemistry 47*, 10526−10539.
(27) Siddiqua, A., and Margittai, M. (2010) Three- and four-repeat Tau coassemble into heterogeneous filaments: an implication for Alzheimer disease. *J. Biol. Chem. 285*, 37920−37926.
(28) Dinkel, P. D., Holden, M. R., Matin, N., and Margittai, M. (2015) RNA Binds to Tau Fibrils and Sustains Template-Assisted Growth. *Biochemistry 54*, 4731−4740.
(29) Daebel, V., Chinnathambi, S., Biernat, J., Schwalbe, M., Habenstein, B., Loquet, A., Akoury, E., Tepper, K., Muller, H., Baldus, M., Griesinger, C., Zweckstetter, M., Mandelkow, E., Vijayan, V., and Lange, A. (2012) beta-Sheet Core of Tau Paired Helical Filaments Revealed by Solid-State NMR. *J. Am. Chem. Soc. 134*, 13982−13989.
(30) Barghorn, S., and Mandelkow, E. (2002) Toward a Unified Scheme for the Aggregation of Tau into Alzheimer Paired Helical Filaments†. *Biochemistry 41*, 14885−14896.
(31) Mylonas, E., Hascher, A., Bernado, P., Blackledge, M., Mandelkow, E., and Svergun, D. I. (2008) Domain conformation of tau protein studied by solution small-angle X-ray scattering. *Biochemistry 47*, 10345−10353.
(32) Goode, B. L., Chau, M., Denis, P. E., and Feinstein, S. C. (2000) Structural and functional differences between 3-repeat and 4-repeat tau isoforms. Implications for normal tau function and the onset of neurodegenetative disease. *J. Biol. Chem. 275*, 38182−38189.
(33) Andronesi, O. C., von Bergen, M., Biernat, J., Seidel, K., Griesinger, C., Mandelkow, E., and Baldus, M. (2008) Characterization of Alzheimer's-like paired helical filaments from the core domain of tau protein using solid-state NMR spectroscopy. *J. Am. Chem. Soc. 130*, 5922−5928.
(34) Dinkel, P. D., Siddiqua, A., Huynh, H., Shah, M., and Margittai, M. (2011) Variations in filament conformation dictate seeding barrier between three- and four-repeat tau. *Biochemistry 50*, 4330−4336.
(35) Luo, Y., Dinkel, P., Yu, X., Margittai, M., Zheng, J., Nussinov, R., Wei, G., and Ma, B. (2013) Molecular insights into the reversible formation of tau protein fibrils. *Chem. Commun. 49*, 3582.
(36) Margittai, M., and Langen, R. (2004) Template-assisted filament growth by parallel stacking of tau. *Proc. Natl. Acad. Sci. U. S. A. 101*, 10278−10283.
(37) Margittai, M., and Langen, R. (2006) Side Chain-dependent Stacking Modulates Tau Filament Structure. *J. Biol. Chem. 281*, 37820−37827.
(38) Moore, C. L., Huang, M. H., Robbennolt, S. A., Voss, K. R., Combs, B., Gamblin, T. C., and Goux, W. J. (2011) Secondary nucleating sequences affect kinetics and thermodynamics of tau aggregation. *Biochemistry 50*, 10876−10886.
(39) Siddiqua, A., Luo, Y., Meyer, V., Swanson, M. A., Yu, X., Wei, G., Zheng, J., Eaton, G. R., Ma, B., Nussinov, R., Eaton, S. S., and Margittai, M. (2012) Conformational Basis for Asymmetric Seeding Barrier in Filaments of Three- and Four-Repeat Tau. *J. Am. Chem. Soc. 134*, 10271−10278.
(40) Yu, X., Luo, Y., Dinkel, P., Zheng, J., Wei, G., Margittai, M., Nussinov, R., and Ma, B. (2012) Cross-seeding and conformational selection between three- and four-repeat human Tau proteins. *J. Biol. Chem. 287*, 14950−14959.
(41) Pouplana, S., Espargaro, A., Galdeano, C., Viayna, E., Sola, I., Ventura, S., Munoz-Torrero, D., and Sabate, R. (2014) Thioflavin-S Staining of Bacterial Inclusion Bodies for the Fast, Simple, and Inexpensive Screening of Amyloid Aggregation Inhibitors. *Curr. Med. Chem. 21*, 1152−1159.
(42) Kuret, J., Congdon, E. E., Li, G., Yin, H., Yu, X., and Zhong, Q. (2005) Evaluating triggers and enhancers of tau fibrillization. *Microsc. Res. Tech. 67*, 141−155.
(43) Lippens, G., Sillen, A., Landrieu, I., Amniai, L., Sibille, N., Barbier, P., Leroy, A., Hanoulle, X., and Wieruszeski, J. M. (2007) Tau aggregation in Alzheimer's disease: what role for phosphorylation? *Prion 1*, 21−25.
(44) Wischik, C. M., Novak, M., Edwards, P. C., Klug, A., Tichelaar, W., and Crowther, R. A. (1988) Structural characterization of the core of the paired helical filament of Alzheimer disease. *Proc. Natl. Acad. Sci. U. S. A. 85*, 4884−4888.
(45) Brion, J. P., Hanger, D. P., Bruce, M. T., Couck, A. M., Flament-Durand, J., and Anderton, B. H. (1991) Tau in Alzheimer neurofibrillary tangles. N- and C-terminal regions are differentially associated with paired helical filaments and the location of a putative abnormal phosphorylation site. *Biochem. J. 273*, 127−133.
(46) Geng, J., Xia, L., Li, W., and Dou, F. (2015) The C-Terminus of Tau Protein Plays an Important Role in Its Stability and Toxicity. *J. Mol. Neurosci. 55*, 251−259.
(47) Gamblin, T. C., Berry, R. W., and Binder, L. I. (2003) Tau Polymerization: Role of the Amino Terminus†. *Biochemistry 42*, 2252−2257.
(48) Horowitz, P. M., LaPointe, N., Guillozet-Bongaarts, A. L., Berry, R. W., and Binder, L. I. (2006) N-Terminal Fragments of Tau Inhibit Full-Length Tau Polymerization in Vitro†. *Biochemistry 45*, 12859−12866.
(49) Yanagawa, H., Chung, S.-H., Ogawa, Y., Sato, K., Shibata-Seki, T., Masai, J., and Ishiguro, K. (1998) Protein Anatomy: C-Tail Region of Human Tau Protein as a Crucial Structural Element in Alzheimer's Paired Helical Filament Formationin Vitro. *Biochemistry 37*, 1979−1988.
(50) Wang, J. Z., Xia, Y. Y., Grundke-Iqbal, I., and Iqbal, K. (2013) Abnormal hyperphosphorylation of tau: sites, regulation, and molecular mechanism of neurofibrillary degeneration. *J. Alzheimers Dis 33*, S123−S139.
(51) Stoothoff, W. H., and Johnson, G. V. (2005) Tau phosphorylation: physiological and pathological consequences. *Biochim. Biophys. Acta, Mol. Basis Dis. 1739*, 280−297.
(52) Kuret, J., Congdon, E. E., Li, G., Yin, H., Yu, X., and Zhong, Q. (2005) Evaluating triggers and enhancers of tau fibrillization. *Microsc. Res. Tech. 67*, 141−155.
(53) Kopke, E., Tung, Y. C., Shaikh, S., Alonso, A. C., Iqbal, K., and Grundke-Iqbal, I. (1993) Microtubule-associated protein tau. Abnormal phosphorylation of a non-paired helical filament pool in Alzheimer disease. *J. Biol. Chem. 268*, 24374−24384.

DOI: 10.1021/acschemneuro.5b00294
ACS Chem. Neurosci. 2016, 7, 565−575

(54) Hanger, D. P., Byers, H. L., Wray, S., Leung, K. Y., Saxton, M. J., Seereeram, A., Reynolds, C. H., Ward, M. A., and Anderton, B. H. (2007) Novel phosphorylation sites in tau from Alzheimer brain support a role for casein kinase 1 in disease pathogenesis. *J. Biol. Chem. 282*, 23645−23654.
(55) Jho, Y. S., Zhulina, E. B., Kim, M. W., and Pincus, P. A. (2010) Monte Carlo Simulations of Tau Proteins: Effect of Phosphorylation. *Biophys. J. 99*, 2387−2397.
(56) Lyons, A. J., Gandhi, N. S., and Mancera, R. L. (2014) Molecular dynamics simulation of the phosphorylation-induced conformational changes of a tau peptide fragment. *Proteins: Struct., Funct., Genet. 82*, 1907−1923.
(57) Luo, Y., Ma, B., Nussinov, R., and Wei, G. (2014) Structural Insight into Tau Protein's Paradox of Intrinsically Disordered Behavior, Self-Acetylation Activity, and Aggregation. *J. Phys. Chem. Lett. 5*, 3026−3031.
(58) Ganguly, P., Do, T. D., Larini, L., LaPointe, N. E., Sercel, A. J., Shade, M. F., Feinstein, S. C., Bowers, M. T., and Shea, J.-E. (2015) Tau Assembly: The Dominant Role of PHF6 (VQIVYK) in Microtubule Binding Region Repeat R3. *J. Phys. Chem. B 119*, 4582−4593.
(59) Wegmann, S., Jung, Y. J., Chinnathambi, S., Mandelkow, E. M., Mandelkow, E., and Muller, D. J. (2010) Human Tau Isoforms Assemble into Ribbon-like Fibrils That Display Polymorphic Structure and Stability. *J. Biol. Chem. 285*, 27302−27313.
(60) Horowitz, P. M., LaPointe, N., Guillozet-Bongaarts, A. L., Berry, R. W., and Binder, L. I. (2006) N-terminal fragments of tau inhibit full-length tau polymerization in vitro. *Biochemistry 45*, 12859−12866.
(61) Reddy, H., Duka, V., Lee, J.-H., Credle, J., Wills, J., Oaks, A., Smolinsky, C., Shah, K., Mash, D. C., Masliah, E., and Sidhu, A. (2013) Identification of the Sites of Tau Hyperphosphorylation and Activation of Tau Kinases in Synucleinopathies and Alzheimer's Diseases. *PLoS One 8*, e75025.
(62) Jellinger, K. A. (2012) Interaction between pathogenic proteins in neurodegenerative disorders. *J. Cell Mol. Med. 16*, 1166−1183.
(63) Gilley, J., Adalbert, R., and Coleman, M. P. (2011) Modelling early responses to neurodegenerative mutations in mice. *Biochem. Soc. Trans. 39*, 933−938.
(64) Moore, C. L., Huang, M. H., Robbennolt, S. A., Voss, K. R., Combs, B., Gamblin, T. C., and Goux, W. J. (2011) Secondary Nucleating Sequences Affect Kinetics and Thermodynamics of Tau Aggregation. *Biochemistry 50*, 10876−10886.
(65) Qi, R., Luo, Y., Wei, G., Nussinov, R., and Ma, B. (2015) Aβ "Stretching-and-Packing" Cross-Seeding Mechanism Can Trigger Tau Protein Aggregation. *J. Phys. Chem. Lett. 6*, 3276−3282.
(66) Goedert, M., Jakes, R., Spillantini, M. G., Hasegawa, M., Smith, M. J., and Crowther, R. A. (1996) Assembly of microtubule-associated protein tau into Alzheimer-like filaments induced by sulphated glycosaminoglycans. *Nature 383*, 550−553.
(67) Abraha, A., Ghoshal, N., Gamblin, T. C., Cryns, V., Berry, R. W., Kuret, J., and Binder, L. I. (2000) C-terminal inhibition of tau assembly in vitro and in Alzheimer's disease. *J. Cell Sci. 113*, 3737−3745.
(68) Xu, L., Nussinov, R., and Ma, B. (2016) Allosteric stabilization of the amyloid-beta peptide hairpin by the fluctuating N-terminal. *Chem. Commun. (Cambridge, U. K.) 52*, 1733−1736.
(69) Berry, R. W., Abraha, A., Lagalwar, S., LaPointe, N., Gamblin, T. C., Cryns, V. L., and Binder, L. I. (2003) Inhibition of tau polymerization by its carboxy-terminal caspase cleavage fragment. *Biochemistry 42*, 8325−8331.
(70) Gamblin, T. C., Chen, F., Zambrano, A., Abraha, A., Lagalwar, S., Guillozet, A. L., Lu, M., Fu, Y., Garcia-Sierra, F., LaPointe, N., Miller, R., Berry, R. W., Binder, L. I., and Cryns, V. L. (2003) Caspase cleavage of tau: linking amyloid and neurofibrillary tangles in Alzheimer's disease. *Proc. Natl. Acad. Sci. U. S. A. 100*, 10032−10037.
(71) Guillozet-Bongaarts, A. L., Garcia-Sierra, F., Reynolds, M. R., Horowitz, P. M., Fu, Y., Wang, T., Cahill, M. E., Bigio, E. H., Berry, R. W., and Binder, L. I. (2005) Tau truncation during neurofibrillary tangle evolution in Alzheimer's disease. *Neurobiol. Aging 26*, 1015−1022.
(72) Lapointe, N. E., Horowitz, P. M., Guillozet-Bongaarts, A. L., Silva, A., Andreadis, A., and Binder, L. I. (2009) Tau 6D and 6P isoforms inhibit polymerization of full-length tau in vitro. *Biochemistry 48*, 12290−12297.
(73) Mondragon-Rodriguez, S., Basurto-Islas, G., Santa-Maria, I., Mena, R., Binder, L. I., Avila, J., Smith, M. A., Perry, G., and Garcia-Sierra, F. (2008) Cleavage and conformational changes of tau protein follow phosphorylation during Alzheimer's disease. *Int. J. Exp. Pathol. 89*, 81−90.
(74) Garcia-Sierra, F., Ghoshal, N., Quinn, B., Berry, R. W., and Binder, L. I. (2003) Conformational changes and truncation of tau protein during tangle evolution in Alzheimer's disease. *J. Alzheimer's Dis. 5*, 65−77.
(75) Gamblin, T. C., Berry, R. W., and Binder, L. I. (2003) Tau polymerization: role of the amino terminus. *Biochemistry 42*, 2252−2257.
(76) Han, W., and Schulten, K. (2012) Further Optimization of a Hybrid United-Atom and Coarse-Grained Force Field for Folding Simulations: Improved Backbone Hydration and Interactions between Charged Side Chains. *J. Chem. Theory Comput. 8*, 4413−4424.
(77) Han, W., Wan, C.-K., Jiang, F., and Wu, Y.-D. (2010) PACE Force Field for Protein Simulations. 1. Full Parameterization of Version 1 and Verification. *J. Chem. Theory Comput. 6*, 3373−3389.
(78) Han, W., Wan, C.-K., and Wu, Y.-D. (2010) PACE Force Field for Protein Simulations. 2. Folding Simulations of Peptides. *J. Chem. Theory Comput. 6*, 3390−3402.
(79) Han, W., and Wu, Y.-D. (2007) Coarse-Grained Protein Model Coupled with a Coarse-Grained Water Model: Molecular Dynamics Study of Polyalanine-Based Peptides. *J. Chem. Theory Comput. 3*, 2146−2161.
(80) Jang, H., Connelly, L., Arce, F. T., Ramachandran, S., Kagan, B. L., Lal, R., and Nussinov, R. (2013) Mechanisms for the Insertion of Toxic, Fibril-like beta-Amyloid Oligomers into the Membrane. *J. Chem. Theory Comput. 9*, 822−833.
(81) Han, W., and Schulten, K. (2014) Fibril Elongation by Aβ17−42: Kinetic Network Analysis of Hybrid-Resolution Molecular Dynamics Simulations. *J. Am. Chem. Soc. 136*, 12450−12460.
(82) Phillips, J. C., Braun, R., Wang, W., Gumbart, J., Tajkhorshid, E., Villa, E., Chipot, C., Skeel, R. D., Kale, L., and Schulten, K. (2005) Scalable molecular dynamics with NAMD. *J. Comput. Chem. 26*, 1781−1802.
(83) Lazaridis, T., and Karplus, M. (1999) Effective energy function for proteins in solution. *Proteins: Struct., Funct., Genet. 35*, 133−152.
(84) Lazaridis, T., and Karplus, M. (1999) Discrimination of the native from misfolded protein models with an energy function including implicit solvation. *J. Mol. Biol. 288*, 477−487.
(85) Lazaridis, T. (1997) "New View" of Protein Folding Reconciled with the Old Through Multiple Unfolding Simulations. *Science 278*, 1928−1931.
(86) Wu, X., and Brooks, B. R. (2003) Self-guided Langevin dynamics simulation method. *Chem. Phys. Lett. 381*, 512−518.
(87) Wu, X., Damjanovic, A., and Brooks, B. R. (2012) Efficient and Unbiased Sampling of Biomolecular Systems in the Canonical Ensemble. *A Review of Self-Guided Langevin Dynamics*, 255−326.
(88) Best, R. B., Zhu, X., Shim, J., Lopes, P. E. M., Mittal, J., Feig, M., and MacKerell, A. D. (2012) Optimization of the Additive CHARMM All-Atom Protein Force Field Targeting Improved Sampling of the Backbone ϕ, ψ and Side-Chain χ1and χ2Dihedral Angles. *J. Chem. Theory Comput. 8*, 3257−3273.
(89) Lee, H. S., Lee, S. N., Joo, C. H., Lee, H., Lee, H. S., Yoon, S. Y., Kim, Y. K., and Choe, H. (2007) Contributions of 3′-overhang to the dissociation of small interfering RNAs from the PAZ domain: Molecular dynamics simulation study. *J. Mol. Graphics Modell. 25*, 784−793.
(90) Brooks, B. R., Brooks, C. L., Mackerell, A. D., Nilsson, L., Petrella, R. J., Roux, B., Won, Y., Archontis, G., Bartels, C., Boresch, S., Caflisch, A., Caves, L., Cui, Q., Dinner, A. R., Feig, M., Fischer, S., Gao,

DOI: 10.1021/acschemneuro.5b00294
ACS Chem. Neurosci. 2016, 7, 565−575

J., Hodoscek, M., Im, W., Kuczera, K., Lazaridis, T., Ma, J., Ovchinnikov, V., Paci, E., Pastor, R. W., Post, C. B., Pu, J. Z., Schaefer, M., Tidor, B., Venable, R. M., Woodcock, H. L., Wu, X., Yang, W., York, D. M., and Karplus, M. (2009) CHARMM: The Biomolecular Simulation Program. *J. Comput. Chem. 30*, 1545−1614.
(91) Thirumalai, D., Reddy, G., and Straub, J. E. (2012) Role of Water in Protein Aggregation and Amyloid Polymorphism. *Acc. Chem. Res. 45*, 83−92.
(92) Fichou, Y., Schirò, G., Gallat, F.-X., Laguri, C., Moulin, M., Combet, J., Zamponi, M., Härtlein, M., Picart, C., Mossou, E., Lortat-Jacob, H., Colletier, J.-P., Tobias, D. J., and Weik, M. (2015) Hydration water mobility is enhanced around tau amyloid fibers. *Proc. Natl. Acad. Sci. U. S. A. 112*, 6365−6370.
(93) Zheng, J., Baghkhanian, A. M., and Nowick, J. S. (2013) A Hydrophobic Surface Is Essential To Inhibit the Aggregation of a Tau-Protein-Derived Hexapeptide. *J. Am. Chem. Soc. 135*, 6846−6852.
(94) Mackerell, A. D., Jr., Feig, M., and Brooks, C. L., III. (2004) Extending the treatment of backbone energetics in protein force fields: limitations of gas-phase quantum mechanics in reproducing protein conformational distributions in molecular dynamics simulations. *J. Comput. Chem. 25*, 1400−1415.
(95) MacKerell, A. D., Bashford, D., Bellott, M., Dunbrack, R. L., Evanseck, J. D., Field, M. J., Fischer, S., Gao, J., Guo, H., Ha, S., Joseph-McCarthy, D., Kuchnir, L., Kuczera, K., Lau, F. T. K., Mattos, C., Michnick, S., Ngo, T., Nguyen, D. T., Prodhom, B., Reiher, W. E., Roux, B., Schlenkrich, M., Smith, J. C., Stote, R., Straub, J., Watanabe, M., Wiórkiewicz-Kuczera, J., Yin, D., and Karplus, M. (1998) All-Atom Empirical Potential for Molecular Modeling and Dynamics Studies of Proteins†. *J. Phys. Chem. B 102*, 3586−3616.
(96) Mark, P., and Nilsson, L. (2001) Structure and Dynamics of the TIP3P, SPC, and SPC/E Water Models at 298 K. *J. Phys. Chem. A 105*, 9954−9960.
(97) Phillips, J. C., Braun, R., Wang, W., Gumbart, J., Tajkhorshid, E., Villa, E., Chipot, C., Skeel, R. D., Kalé, L., and Schulten, K. (2005) Scalable molecular dynamics with NAMD. *J. Comput. Chem. 26*, 1781−1802.
(98) Lee, M. S., Feig, M., Salsbury, F. R., and Brooks, C. L. (2003) New analytic approximation to the standard molecular volume definition and its application to generalized Born calculations. *J. Comput. Chem. 24*, 1348−1356.
(99) Brooks, B. R., Bruccoleri, R. E., Olafson, B. D., States, D. J., Swaminathan, S., and Karplus, M. (1983) CHARMM: A program for macromolecular energy, minimization, and dynamics calculations. *J. Comput. Chem. 4*, 187−217.

DOI: 10.1021/acschemneuro.5b00294
ACS Chem. Neurosci. 2016, 7, 565−575